

SCIENTIFIC REPORTS

OPEN

Orbital Delocalization and Enhancement of Magnetic Interactions in Perovskite Oxyhydrides

Kai Liu, Yusheng Hou, Xingao Gong & Hongjun Xiang

Received: 15 September 2015

Accepted: 16 November 2015

Published: 25 January 2016

Recent experiments showed that some perovskite oxyhydrides have surprisingly high magnetic-transition temperature. In order to unveil the origin of this interesting phenomenon, we investigate the magnetism in SrCrO_2H and SrVO_2H on the basis of first-principles calculations and Monte Carlo simulations. Our work indicates that the Cr-O-Cr superexchange interaction in SrCrO_2H is unexpectedly strong. Different from the previous explanation in terms of the H^- ion substitution induced increase of the Cr-O-Cr bond angle, we reveal instead that this is mainly because the $3d$ orbitals in perovskite oxyhydrides becomes more delocalized since H^- ions have weaker electronegativity and less electrons than O^{2-} ions. The delocalized $3d$ orbitals result in stronger Cr-O interactions and enhance the magnetic-transition temperature. This novel mechanism is also applicable to the case of SrVO_2H . Furthermore, we predict that SrFeO_2H will have unprecedented high Neel temperature because of the extraordinarily strong Fe-H-Fe σ -type interactions. Our work suggests the anion substitution can be used to effectively manipulate the magnetic properties of perovskite compounds.

Complex transition metal oxides have been the subject of enduring interest due to the wide variety of physical properties they exhibit, to name a few, high- T_c superconductivity, magnetoresistance, multiferroicity, thermoelectric response, and so on¹⁻⁷. For the past few years, scientists have found that replacing segmental O^{2-} ions in transition metal oxides by N^{3-} , F^- or S^{2-} can result in novel materials such as pigments, water-splitting photocatalysis, dielectric and cathode material⁸⁻¹². Different from N^{3-} , F^- or S^{2-} which has p valence electrons, the H^- anion has a filled $1s^2$ electronic configuration that is fundamentally different from the O^{2-} ion case. Therefore, it is expected that the H^- ion substitution might leads to exotic behaviors in perovskite. In pioneering works, a large amount of hydrogen species were incorporated into ATiO_3 ($A = \text{Ba}, \text{Sr}, \text{Ca}$) and Sr_2VO_4 lattice through the use of CaH_2 reductant¹³⁻¹⁶. The resulting oxyhydride $\text{ATiO}_{3-x}\text{H}_x$ exhibits high electronic conductivity and its hydride ions are exchangeable with gaseous hydrogen at elevated temperature, indicating that it can be an ideal mixed electron/hydride proton conductor for electrochemical applications¹³⁻¹⁵. In oxyhydride $\text{Sr}_2\text{VO}_{4-x}\text{H}_x$, the hydride ion could act as an effective carrier dopant because the hydrogen and oxygen concentrations can be controlled¹⁶.

Interestingly, it was experimentally found that the magnetic properties of transition metal oxides may change dramatically if some oxygen anions are replaced by hydrogen anions. An antiferromagnetic-to-ferromagnetic transition in $\text{EuTiO}_{3-x}\text{H}_x$ induced by hydride substitution was reported, where the ferromagnetism was caused by the Ruderman-Kittel-Kasuya-Yosida (RKKY) interaction between the Eu^{2+} spins mediated by the itinerant Ti $3d$ electrons¹⁷. $\text{LaSrCoO}_3\text{H}_{0.7}$ ¹⁸⁻²⁰ and $\text{Sr}_3\text{Co}_2\text{O}_{4.33}\text{H}_{0.84}$ ²¹ were found to display high magnetic transition temperatures. Recently, the stoichiometric perovskite oxyhydrides SrCrO_2H and SrVO_2H have been synthesized^{22,23}. The average structure of SrCrO_2H is the cubic perovskite where the hydride ions are randomly distributed. In SrVO_2H , the planar VO_2 layers are connected by hydride ions. The experimentally observed antiferromagnetic (AFM) Neel temperature (T_N) of SrCrO_2H and SrVO_2H are around 380 K and higher than 300 K^{22,23}, respectively. It is puzzling that the Neel temperature T_N of SrCrO_2H is higher than that (290 K)^{24,25} of LaCrO_3 . In both SrCrO_2H and LaCrO_3 , the valence of Cr element is $3+$ with the three $3d$ electrons occupying the t_{2g} orbitals, that

Key Laboratory of Computational Physical Sciences (Ministry of Education), State Key Laboratory of Surface Physics, Collaborative Innovation Center of Advanced Microstructures, and Department of Physics, Fudan University, Shanghai 200433, P.R. China. Correspondence and requests for materials should be addressed to H.X. (email: hxjiang@fudan.edu.cn)

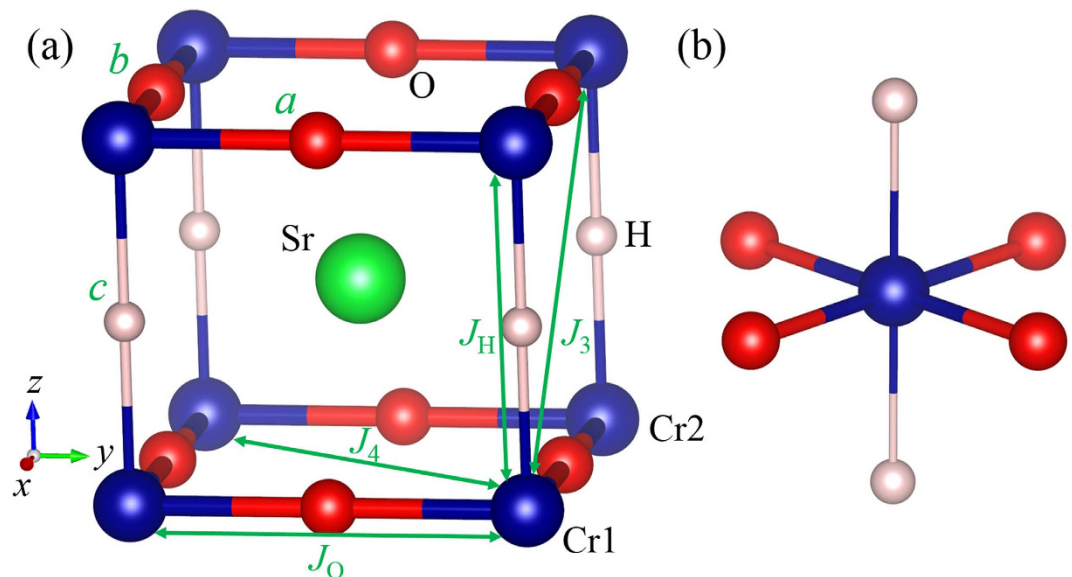


Figure 1. (a) Perspective view of the ground state structure of SrCrO₂H. The green, blue, red, and greyish spheres represent the Sr²⁺, Cr³⁺, O²⁻, and H⁻ ions, respectively. The spin exchange paths J_0 , J_H , J_3 , and J_4 are also indicated. (b) The local structure of the CrO₄H₂ octahedron.

is, the electron configuration is $(d_{xy})^1(d_{yz})^1(d_{xz})^1$. In average, each Cr³⁺ ion in SrCrO₂H has two Cr-H-Cr superexchange paths and four Cr-O-Cr superexchange paths. Since the t_{2g} orbitals of the Cr³⁺ ion could not interact with the 1s orbitals of H⁻ ions by symmetry, the Cr-H-Cr superexchange interaction is negligible. In LaCrO₃, there are six Cr-O-Cr superexchange paths for each Cr³⁺ ion. So the fact that the Neel temperature T_N of SrCrO₂H is higher than that of LaCrO₃ is rather unexpected.

To probe the origin of the high T_N in SrCrO₂H and SrVO₂H, we studied the magnetic properties of SrCrO₂H, SrVO₂H, and LaCrO₃ based on the density functional theory (DFT). We show that due to weaker electronegativity and less electrons of H⁻ ions than those of O²⁻ ions, the substitution of H⁻ ions with O²⁻ ions lead to more delocalized 3d orbitals of Cr³⁺ ions which make Cr-O-Cr superexchange in SrCrO₂H much stronger and leads to a high T_N . This new mechanism is also applicable to the case of SrVO₂H.

Although the H⁻ ion was experimentally reported to be randomly distributed in SrCrO₂H, we will adopt an ordered structure (see Fig. 1a) to investigate the magnetism in SrCrO₂H for the following reasons. First, by using the cluster expansion approach, we find the ground state structure of SrCrO₂H is similar to the experimentally observed structure of SrVO₂H. Second, we find that the magnetic properties of another SrCrO₂H structure with a more random H⁻ ion distribution are similar to those of the ordered structure (see Supplementary Material). The ground state structure (tetragonal $P4/mmm$ symmetry) of SrCrO₂H has one H⁻ ion and two O²⁻ ions in the primitive cell. The Cr³⁺ cations are located within square planes of oxide ions and form CrO₂ sheets. The CrO₂ sheets are connected by hydride ions, which occupy the remaining two coordination sites around each Cr³⁺ center. Thus the ground state structure of SrCrO₂H can be described by a CrO₂-SrH-CrO₂-SrH stacking sequence. The computed phonon frequencies²⁶ (see Supplementary Figure S3) indicate that the ground state structure of SrCrO₂H is dynamically stable.

To examine the magnetic properties of SrCrO₂H, we considered four ordered spin states, namely, the ferromagnetic (FM), A-type AFM, C-type AFM and G-type AFM states. The experimentally observed AFM structure is the G-type. Our GGA + U calculations show that all the AFM states have lower energy than the FM state, and the G-type AFM is indeed the ground state, in consistent with experimental observations²². To extract the values of the spin exchange parameters, we adopt the four-state mapping approach^{27,28}. There are four relevant Cr-Cr spin exchange interactions (see Fig. 1a): (1) J_0 is the nearest neighbor (NN) superexchange interaction for the Cr-O-Cr path; (2) J_H is the NN spin exchange interaction for the Cr-H-Cr path; (3) J_3 is next nearest neighbor (NNN) super-superexchange interaction in the plane; (4) J_4 is the NNN out of plane super-superexchange interaction. The calculated exchange parameters in the tetragonal structure of SrCrO₂H are summarized in Table 1. As expected, the NN Cr-O-Cr path has the strongest spin exchange interaction (J_0) since it is mediated by the strong π - π hybridization between 3d and 2p orbitals. The NN spin exchange interaction J_H is weakly AFM due to the direct through-space overlap between the t_{2g} orbitals of Cr³⁺ ions. The NNN exchange interactions (J_3 and J_4) are negligible. The AFM nature of the NN interactions can result in the G-type AFM order. Based on the calculated spin exchange parameters, our Monte Carlo (MC) simulations indicate that the T_N is around 285 K. If a smaller Hubbard U is adopted, we can get higher T_N according to the theory of superexchange, in better agreement with the experimentally observed T_N ²².

For comparison, we also studied the magnetism in LaCrO₃. Experiments show the ground state structure of LaCrO₃ is the GdFeO₃-type distorted perovskite with $Pbnm$ space group and its lattice constants are $a = 5.478$, $b = 7.759$, and $c = 5.516$ ²⁹. The lattice constants of our optimized $Pbnm$ structure are $a = 5.468$ Å, $b = 7.758$ Å,

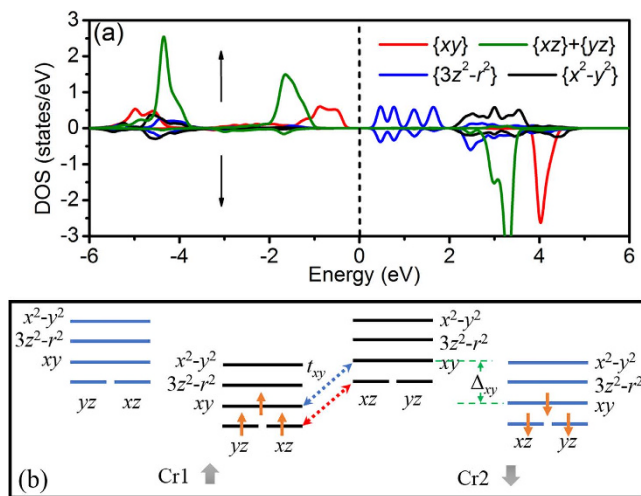


Figure 2. (a) PDOS of the spin-up Cr^{3+} ion in SrCrO_2H with the G-type AFM order. (b) Energy level and electron occupation for the spin-up Cr1 ion and spin-down Cr2 ion. The positions of Cr1 and Cr2 are shown in Fig. 1a. The spin-up and spin-down levels are denoted by black and blue colors, respectively. The effective orbital hoppings responsible for the Cr1-Cr2 superexchange interaction are illustrated.

	J_O (meV)	J_H (meV)	J_3 (meV)	J_4 (meV)	T_N (K)
SrCrO_2H (opt.)	23.95	3.26	-0.96	0.34	285
SrCrO_2H (cubic)	29.69	1.27	-1.26	0.69	325
LaCrO_3 (opt.)	8.88	-	-	0.38	137
LaCrO_3 (cubic)	14.25	-	-	0.73	204
SrVO_2H (opt.)	23.54	1.88	-0.71	0.17	255
SrFeO_2H (opt.)	39.63	89.26	-4.42	4.22	950
SrFeO_2H (cubic)	42.89	70.41	-3.89	-0.91	922

Table 1. Spin exchange parameters and Neel temperature of perovskite systems considered in this work.

In SrCrO_2H , SrVO_2H , and SrFeO_2H , the spin exchange paths J_O , J_H , J_3 , and J_4 are defined in Fig. 1a. Positive (negative) values indicate that the spin exchange interactions are AFM (FM). The exchange parameters are effective by setting the spin magnitude to 1. In LaCrO_3 , J_O is the average NN spin exchange parameter and J_4 is the average NNN spin exchange parameter. “opt.” refers to the structure optimized by GGA + U calculations, while “cubic” refers to the cubic perovskite structure.

and $c = 5.497 \text{ \AA}$, in good agreement with experiment. The obtained spin exchange parameters of the optimized LaCrO_3 are summarized in Table 1. The NN interaction J_O is AFM and the NNN interactions are negligible. This is in accord with the experimentally observed G-type AFM ground state in LaCrO_3 . Compared with SrCrO_2H , it is clear that J_O in LaCrO_3 is much weaker. Based on the calculated spin exchange parameters, our MC simulations indicate that the T_N for LaCrO_3 is around 133 K. Therefore, our theoretical calculations confirm the experimental observation that SrCrO_2H has a higher T_N than LaCrO_3 , as shown in Fig. 3.

Now we begin to understand the difference in the magnetic properties between SrCrO_2H and LaCrO_3 . There are two significant differences between SrCrO_2H and LaCrO_3 . First, there is a structural difference. The CrO_6 octahedron in LaCrO_3 is tilted due to a small tolerance factor, while there is no octahedron tilt in SrCrO_2H . As a result, the Cr-O-Cr angle in SrCrO_2H is 180° while the average Cr-O-Cr angle in LaCrO_3 is 167° . Second, a chemical difference exists since one third of the O^{2-} ions are replaced by H^- ions.

To make clear whether the structural difference or the chemical difference is responsible for the stronger Cr-O-Cr exchange in SrCrO_2H , we investigate the magnetic properties of SrCrO_2H and LaCrO_3 with the same cubic perovskite crystal structure. The lattice constant is set to be the average lattice constant (3.85 \AA) of experimental SrCrO_2H structure²². Note that the hypothetical cubic LaCrO_3 phase can be regarded as a result of substituting Sr^{2+} and H^- in cubic SrCrO_2H with La^{3+} and O^{2-} , respectively. The computed spin exchange parameters of these two cubic structures are summarized in Table 1. Surprisingly and interestingly, the Cr-O-Cr superexchange (29.69 meV) in SrCrO_2H is almost as twice as that (14.25 meV) in LaCrO_3 despite of the fact that the Cr-O bond length and the Cr-O-Cr bond angle are identical in cubic SrCrO_2H and LaCrO_3 . As expected, the Cr-O-Cr exchange in cubic LaCrO_3 is stronger than that (8.88 meV) in $Pbnm$ LaCrO_3 according to the Goodenough-Kanamori rule^{30–32}. Previously, it was suggested that the structural difference is solely responsible for the high T_N in SrCrO_2H ²². However, our calculations show that the structure difference and chemical difference enhance the Cr-O-Cr exchange interaction by 5.37 meV and 15.44 meV, respectively. Therefore, the effect

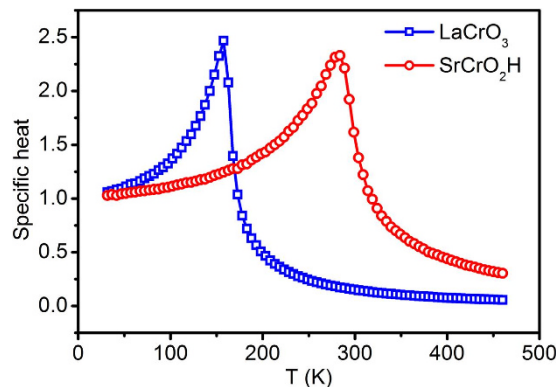


Figure 3. Specific heat of SrCrO₂H and LaCrO₃ calculated as a function of temperature from the MC simulations of the classical spin Hamiltonian.

	t_{xz} (eV)	t_{yz} (eV)	t_{xy} (eV)
SrCrO ₂ H (cubic)	-0.385	0.002	-0.213
LaCrO ₃ (cubic)	-0.217	-0.017	-0.217

Table 2. Effective hopping between the d_{xz} , d_{yz} , d_{xy} orbitals of nearest neighboring Cr ions in cubic SrCrO₂H and LaCrO₃ through the MLWF technique.

of chemical difference on the Cr-Cr exchange interaction is much more important than that of the structural difference.

To account for why J_0 in the cubic SrCrO₂H is as twice as that in the cubic LaCrO₃, we examine their electronic structures in details. Figure 2a shows the partial density of states (PDOS) of the spin-up Cr³⁺ ion in SrCrO₂H with the G-type AFM order. We can see that, for SrCrO₂H, the majority-spin t_{2g} (d_{xy} , d_{xz} , and d_{yz}) orbitals are occupied by three electrons but the majority-spin e_g orbitals are unoccupied, which is similar to the orbital occupation in LaCrO₃. The energy level and occupancy of the 3d orbitals of the tetragonal SrCrO₂H are shown in Fig. 2b. Note that the t_{2g} orbitals split into the low-lying two-fold degenerate d_{xz}/d_{yz} level and a higher d_{xy} level as a result of the tetragonal symmetry.

Without loss of generality, we consider the spin exchange J_0 for the Cr1-O-Cr2 path along the x axis, as shown in Fig. 1a. According to Anderson's superexchange theory³³, the magnitude of the spin exchange can be estimated by t^2/Δ , where t is the effective hopping between the d orbitals and Δ is the energy difference between majority-spin and minority-spin orbitals. In the cubic SrCrO₂H or LaCrO₃, the d_{xz} orbital can only interact with the neighboring d_{xz} orbital, and so do d_{xy} , d_{yz} . The magnitude of J_0 for the Cr1-O-Cr2 path can be estimated as $J_0 \propto t_{xz}^2/\Delta_{xz} + t_{yz}^2/\Delta_{yz} + t_{xy}^2/\Delta_{xy}$, where t_m ($m=xz, yz, xy$) is effective hopping between the m orbitals of Cr1 and Cr2, and Δ_m is the energy difference between the majority-spin m orbital and minority-spin m orbital of the Cr³⁺ ion (see Fig. 2b). The Δ_m parameters are estimated by constructing the maximally localized Wannier functions (MLWFs) based on the ferromagnetic electronic structure. It turns out that Δ_m (about 5.3 eV) in SrCrO₂H is rather close to that (about 5.5 eV) in LaCrO₃. Therefore, we can regard Δ_m as a constant. The effective hopping parameters t_m between the Cr 3d orbitals is obtained by constructing the MLWFs using the spin-unpolarized Bloch wavefunctions. These hopping parameters are listed in Table 2. We can see that the hopping parameter t_{yz} between the d_{yz} orbitals of Cr1 and Cr2 is negligible since these two orbitals are almost parallel to each other. The π - π hopping parameter t_{xy} in the cubic SrCrO₂H are the same as that in the cubic LaCrO₃. The striking result is that the π - π hopping parameter t_{xz} between the d_{xz} orbitals of Cr1 and Cr2 in the cubic SrCrO₂H is almost 50% stronger than that in LaCrO₃. Using these hopping parameters, we can estimate the ratio between J_0 in cubic SrCrO₂H and that in LaCrO₃ as:

$$\frac{J_0(\text{SrCrO}_2\text{H})}{J_0(\text{LaCrO}_3)} = \frac{t_{xz}^2(\text{SrCrO}_2\text{H}) + t_{xy}^2(\text{SrCrO}_2\text{H})}{t_{xz}^2(\text{LaCrO}_3) + t_{xy}^2(\text{LaCrO}_3)} = 2.1.$$

Thus, our first-principles result can be well accounted for by this simple model. This analysis clearly shows that the stronger t_{xz} hopping in SrCrO₂H is responsible for its high T_N .

Figure 4a,b shows the real-space distribution of the d_{xz} -like MLWFs in the cubic SrCrO₂H and LaCrO₃. It is clear that the effective d_{xz} -like MLWF not only distributes around the Cr ion, but also has tails on the neighboring O²⁻ ions due to the anti-bonding π^* hybridization between Cr- d_{xz} and O-2p orbitals. It is the tails on the O²⁻ ions that mediate the effective hopping between the Cr- d_{xz} orbitals. An interesting observation is that the lobes on the O²⁻ ion in the MLWF of SrCrO₂H are bigger than those in LaCrO₃. This suggests that the interaction between Cr- d_{xz} orbital and O- p_z orbital in SrCrO₂H is stronger than that in LaCrO₃, in agreement with our previous result that the effective hopping between the d_{xz} orbitals of Cr1 and Cr2 in SrCrO₂H is larger than that in LaCrO₃.

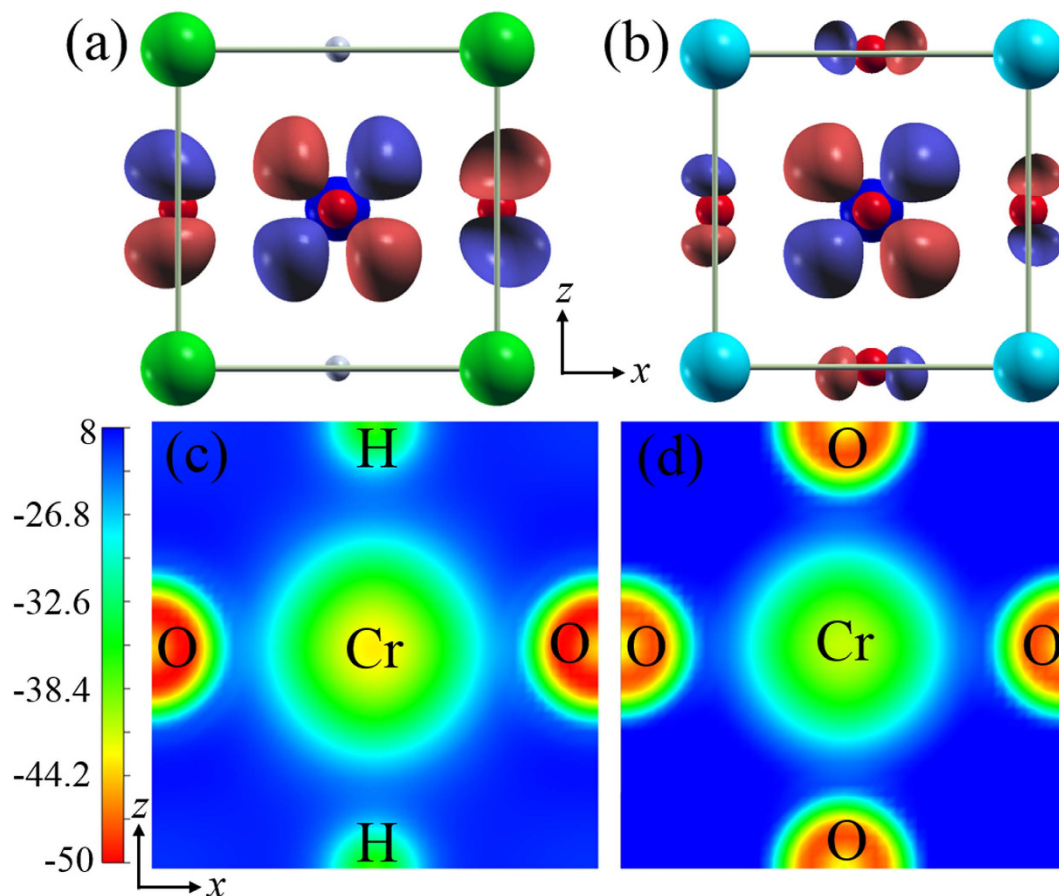


Figure 4. Isosurface plots of the Cr- d_{xz} like MLWFs for (a) cubic SrCrO₂H and (b) cubic LaCrO₃. The lobes on the O²⁻ ion in the MLWF of SrCrO₂H are bigger than those of LaCrO₃, indicating that the hybridization between Cr- d_{xz} orbital and O- p_z is stronger in SrCrO₂H. Contour plots of the electrostatic potential in (c) cubic SrCrO₂H and (d) cubic LaCrO₃, projected on the xz -plane passing through Cr, H, and O sites. The electrostatic potential along the Cr-H direction is much weaker than that along the Cr-O direction in SrCrO₂H.

We propose that the stronger interaction between Cr- d_{xz} orbital and O- p_z orbital in SrCrO₂H results from the more delocalized Cr- d_{xz} orbital in SrCrO₂H (see Supplementary Figure S5). This is supported by a separate MLWF analysis which indicates that the spread of the atomic Cr- d_{xz} orbital in the cubic SrCrO₂H is larger than that in the cubic LaCrO₃. The more delocalized Cr- d_{xz} orbital in SrCrO₂H can be reasoned by considering the electrostatic potential exerted on the Cr 3d electrons. The contour plots of the electrostatic potential on the xz -plane are displayed in the Fig. 4c,d. We can see that the electrostatic potential along the Cr-H direction is much weaker than that along the Cr-O direction. Thus, the d_{xz} orbital in SrCrO₂H is more delocalized along the z -axis, as can also be seen from Fig. 4a. It is the weaker repulsion between the H⁻ ion and the 3d electrons that makes the d_{xz} orbital in SrCrO₂H more delocalized. The weaker electrostatic potential along the Cr-H direction results from the fact that H⁻ ions have the weaker electronegativity and less charge than O²⁻ ions. Therefore, the replacement of O²⁻ ions by H⁻ ions will not only change the hybridization type between the transition metal and the anions, but also affect the wavefunction distribution of d orbitals. Such novel mechanism revealed here for SrCrO₂H can be also applied to SrVO₂H. The only difference is that there is one d electron less than that in SrCrO₂H, which makes the T_N slightly lower (see Supplementary Material). We note that first-principles calculations³⁴ were recently carried out to study the electronic and magnetic properties of SrVO₂H. However, the mechanism for the high Neel temperature in SrVO₂H was not discovered.

The mechanism that the H⁻ ion induced delocalization of the d orbitals is general and may have profound effect on the electronic and magnetic properties of other perovskite oxyhydrides. Below we will predict that SrFeO₂H has an extremely high T_N . With the cluster expansion approach, we predict that SrFeO₂H takes the same ground state structure as that of SrCrO₂H. This is reasonable since the ionic radius of the Fe³⁺ ion is close to that of the Cr³⁺ ion. The optimized lattice constants a and c for SrFeO₂H are 3.997 Å and 3.645 Å, respectively. The computed phonon dispersion²⁶ (see Supplementary Figure S4) indicates that SrFeO₂H is dynamically stable. The spin exchange parameters calculated for the optimized SrFeO₂H structures are listed in Table 1. SrFeO₂H takes the G-type AFM order as the magnetic ground state since the NN AFM spin exchanges J_O (Fe-O-Fe) and J_H (Fe-H-Fe) are dominant. To our surprise, the spin exchange J_H (89.26 meV) in SrFeO₂H is much stronger than J_O (39.63 meV) in SrFeO₂H. Note that the much stronger Fe-H-Fe interaction is not mainly caused by the shorter Fe-H distance than the Fe-O distance, because similar results are also obtained in the cubic perovskite SrFeO₂H

structure. In fact, the much stronger Fe-H-Fe interaction is mainly because the out-of-plane Fe- $d_{3z^2-r^2}$ orbital is more delocalized than the in-plane Fe- $d_{3x^2-r^2}$ and $d_{3y^2-r^2}$ orbitals. Therefore, the σ bond between the H 1s orbital and Fe- $d_{3z^2-r^2}$ orbital is much stronger than the σ bond between the O-2p orbitals and the in-plane Fe $d_{3x^2-r^2}/d_{3y^2-r^2}$ orbitals (see Supplementary Figure S6). Similar to the cases of SrCrO₂H and SrVO₂H, the weaker electrostatic potential of H⁻ ions exerting on the d electrons of Fe³⁺ ions leads to more delocalized Fe- $d_{3z^2-r^2}$ orbitals, which results in an anomalously strong spin exchange J_{H} . Our MC simulations indicate that the T_{N} of SrFeO₂H is around 826 K, which is even higher than that of BiFeO₃ ($T_{\text{N}} = 643$ K)³⁵ and SrFeO₂ with a quasi-two-dimensional structure ($T_{\text{N}} = 473$ K)^{36,37}. Our result suggests that the replacement of O²⁻ ions by H⁻ ions can enhance the magnetic interactions not only in t_{2g} d^2 and d^3 systems, but also in d^5 systems. Our work suggests that the high magnetic transition temperature in LaSrCoO₃H_{0.7}^{18–20} and Sr₃Co₂O_{4.33}H_{0.84}²¹ should be also due to the H⁻ ion induced delocalization of the $3d$ e_g orbitals.

In summary, we perform a systematic theoretical study on the magnetic properties of perovskite oxyhydrides. The high magnetic transition temperature in SrCrO₂H is revealed to be due to the delocalization of $3d$ orbitals in perovskite oxyhydrides. This is because H⁻ ions have weaker electronegativity and fewer electrons than O²⁻ ions. The more delocalized $3d$ orbitals in SrCrO₂H make Cr-O-Cr superexchange strong and T_{N} high. This novel mechanism also applies to the case of SrVO₂H. We predict that the σ -type Fe-H-Fe interactions in SrFeO₂H are extraordinarily strong which also result from the delocalization of the $3d$ orbitals. The delocalization of d orbitals in oxyhydrides discovered in this work is universal and may also have profound effects on properties other than the magnetic properties.

Methods

Our DFT calculations are performed on the basis of the projector augmented wave method^{38,39} encoded in the Vienna ab initio simulation package^{40,41} (VASP) using the generalized-gradient approximation (GGA) of Perdew, Burke, and Ernzerhof⁴². The plane-wave cutoff energy is set to be 450 eV. To properly describe the strong electron correlation in the $3d$ transition-metal oxide, the GGA plus on-site repulsion U method (GGA + U) is employed⁴³. $U = 4$ eV and $J = 1$ eV are applied to the $3d$ electron of Cr³⁺ ions. The maximally localized Wannier functions (MLWFs) are constructed with the Wannier90 program^{44,45}. The spread functional is considered to be converged if the corresponding fractional change because two successive iterations is smaller than 10^{-10} . To find the ground state structures of SrCrO₂H, SrVO₂H, and SrFeO₂H, we adopt the cluster expansion approach⁴⁶ by using the alloy theoretic automation toolkit (ATAT)⁴⁷.

We perform parallel tempering Monte Carlo (PTMC) simulations^{48,49} to estimate the magnetic transition temperature. In PTMC simulations, many replicas with different temperature are simultaneously simulated and a virtual process exchanging configuration of these replicas is introduced. PTMC simulations can avoid a local minimum at low temperatures and can reduce relaxation time. We adopt a $10 \times 10 \times 10$ supercell to perform PTMC simulations. Our test shows that the results obtained with a $12 \times 12 \times 12$ supercell are almost the same as those with the $10 \times 10 \times 10$ supercell. The number of replicas is set to 120.

References

- Okuda, T., Nakanishi, K., Miyasaka, S. & Tokura, Y. Large Thermoelectric Response of Metallic Perovskites: Sr_{1-x}La_xTiO₃ ($0 \leq x \leq 0.1$). *Phys. Rev. B* **63**, 113104 (2001).
- Dagotto, E., Hotta, T. & Moreo, A. Colossal Magnetoresistant Materials: The Key Role of Phase Separation. *Phys. Rep.* **344**, 1–153 (2001).
- Moritomo, Y., Asamitsu, A., Kuwahara, H. & Tokura, Y. Giant Magnetoresistance of Manganese Oxides with a Layered Perovskite Structure. *Nature* **380**, 141–144 (1996).
- Vonhelmolt, R., Wecker, J., Holzapfel, B., Schultz, L. & Samwer, K. Giant Negative Magnetoresistance in Perovskitelike La_{2/3}Ba_{1/3}MnO_x Ferromagnetic Film. *Phys. Rev. Lett.* **71**, 2331–2333 (1993).
- Bednorz, J. G. & Muller, K. A. Possible High T_c Superconductivity in the Ba-La-Cu-O System. *Z. Phys. B: Condens. Matter* **64**, 189–193 (1986).
- Cohen, R. E. Origin of Ferroelectricity in Perovskite Oxides. *Nature* **358**, 136–138 (1992).
- Johnston, D. C., Prakash, H., Zachariasen, W. H. & Viswanathan, R. High Temperature Superconductivity in the Li-Ti-O Ternary System. *Mater. Res. Bull.* **8**, 777–784 (1973).
- Jansen, M. & Letschert, H. P. Inorganic Yellow-Red Pigments without Toxic Metals. *Nature* **404**, 980–982 (2000).
- Kasahara, A. *et al.* Photoreactions on LaTiO₂N under Visible Light Irradiation. *J. Phys. Chem. A* **106**, 6750–6753 (2002).
- Zhang, Y. R., Masubuchi, Y., Motohashi, T., Kikkawa, S. & Hirota, K. Hot Isostatic Press Sintering and Dielectric Properties of SrTaO₂N Ceramics. *Ceram. Int.* **39**, 3377–3380 (2013).
- Zhang, Y.-R., Motohashi, T., Masubuchi, Y. & Kikkawa, S. Sintering and Dielectric Properties of Perovskite SrTaO₂N Ceramics. *J. Eur. Ceram. Soc.* **32**, 1269–1274 (2012).
- Tong, W., Yoon, W. S., Hagh, N. M. & Amatucci, G. G. A Novel Silver Molybdenum Oxyfluoride Perovskite as a Cathode Material for Lithium Batteries. *Chem. Mater.* **21**, 2139–2148 (2009).
- Kobayashi, Y. *et al.* An Oxyhydride of BaTiO₃ Exhibiting Hydride Exchange and Electronic Conductivity. *Nat. Mater.* **11**, 507–511 (2012).
- Sakaguchi, T. *et al.* Oxyhydrides of (Ca,Sr,Ba)TiO₃ Perovskite Solid Solutions. *Inorg. Chem.* **51**, 11371–11376 (2012).
- Yajima, T. *et al.* Epitaxial Thin Films of ATiO_{3-x}H_x (A = Ba, Sr, Ca) with Metallic Conductivity. *J. Am. Chem. Soc.* **134**, 8782–8785 (2012).
- Bang, J. *et al.* Hydrogen Ordering and New Polymorph of Layered Perovskite Oxyhydrides: Sr₂VO_{4-x}H_x. *J. Am. Chem. Soc.* **136**, 7221–7224 (2014).
- Yamamoto, T. *et al.* An Antiferro-to-Ferromagnetic Transition in EuTiO_{3-x}H_x Induced by Hydride Substitution. *Inorg. Chem.* **54**, 1501–1507 (2015).
- Blundell, S. J. *et al.* Magnetism in Oxide Chains Bridged with the Hydride Anion: LaSrCoO₃H_{0.7} Studied Using Muon-Spin Rotation. *Physica B* **326**, 527–531 (2003).
- Bridges, C. A., Darling, G. R., Hayward, M. A. & Rosseinsky, M. J. Electronic Structure, Magnetic Ordering, and Formation Pathway of the Transition Metal Oxide Hydride LaSrCoO₃H_{0.7}. *J. Am. Chem. Soc.* **127**, 5996–6011 (2005).
- Hayward, M. A. *et al.* The Hydride Anion in an Extended Transition Metal Oxide Array: LaSrCoO₃H_{0.7}. *Science* **295**, 1882–1884 (2002).

21. Helps, R. M., Rees, N. H. & Hayward, M. A. $\text{Sr}_3\text{Co}_2\text{O}_{4.33}\text{H}_{0.84}$: an Extended Transition Metal Oxide-Hydride. *Inorg. Chem.* **49**, 11062–11068 (2010).
22. Tassel, C. *et al.* Direct Synthesis of Chromium Perovskite Oxyhydride with a High Magnetic-Transition Temperature. *Angew. Chem. Int. Ed.* **53**, 10377–10380 (2014).
23. Romero, F. D. *et al.* Strontium Vanadium Oxide-Hydrides: “Square-Planar” Two-Electron Phases. *Angew. Chem. Int. Ed.* **53**, 7556–7559 (2014).
24. Aleonard, R., Pauthene, R., Rebouill, J. P. & Veyret, C. Interpretation of the Magnetic Properties of the Rare Earth Chromites and the Rare Earth Manganites. *J. Appl. Phys.* **39**, 379 (1968).
25. Weinberg, I. & Larssen, P. Electron Paramagnetic Resonance and Antiferromagnetism in LaCrO_3 . *Nature* **192**, 445–446 (1961).
26. Togo, A., Oba, F. & Tanaka, I. First-Principles calculations of the ferroelastic transition between rutile-type and CaCl_2 -type SiO_2 at high pressures. *Phys. Rev. B* **78**, 134106 (2008).
27. Xiang, H. J., Kan, E. J., Wei, S.-H., Whangbo, M. H. & Gong, X. G. Predicting the Spin-Lattice Order of Frustrated Systems from First Principles. *Phys. Rev. B* **84**, 224429 (2011).
28. Xiang, H., Lee, C., Koo, H. J., Gong, X. & Whangbo, M. H. Magnetic Properties and Energy-Mapping Analysis. *Dalton. Trans.* **42**, 823–853 (2013).
29. Mitchell, R. H. & Chakhmouradian, A. R. A New Series of Complex Perovskites $\text{La}_{1-x}\text{Sr}_x\text{Cr}_{1-x}\text{Ti}_x\text{O}_3$: Structural Characterization. *J. Solid State Chem.* **144**, 81–85 (1999).
30. Goodenough, J. B., Wickham, D. G. & Croft, W. J. Some Magnetic and Crystallographic Properties of the System $\text{Li}_x\text{Ni}^{2+}_{1-2x}\text{Ni}^{3+}_x\text{O}$. *J. Phys. Chem. Solids* **5**, 107–116 (1958).
31. Kanamori, J. Theory of the Magnetic Properties of Ferrous and Cobaltous Oxides, I. *Prog. Theor. Phys.* **17**, 177–196 (1957).
32. Kanamori, J. Theory of the Magnetic Properties of Ferrous and Cobaltous Oxides, II. *Prog. Theor. Phys.* **17**, 197–222 (1957).
33. Anderson, P. W. Antiferromagnetism - Theory of Superexchange Interaction. *Phys. Rev.* **79**, 350–356 (1950).
34. Wei, Y. *et al.* The Effect of Hydrogen Ordering on the Electronic and Magnetic Properties of the Strontium Vanadium Oxyhydride. *J. Phys. Condens. Matter.* **27**, 206001 (2015).
35. Wang, J. *et al.* Epitaxial BiFeO_3 Multiferroic Thin Film Heterostructures. *Science* **299**, 1719–1722 (2003).
36. Tsujimoto, Y. *et al.* Infinite-layer iron oxide with a square-planar coordination. *Nature* **450**, 1062–1065 (2007).
37. Xiang, H. J., Wei, S.-H. & Whangbo, M. H. Origin of the Structural and Magnetic Anomalies of the Layered Compound SrFeO_2 : A Density Functional Investigation. *Phys. Rev. Lett.* **100**, 167207 (2008).
38. Blöchl, P. E. Projector augmented-wave method. *Phys. Rev. B* **50**, 17953–17979 (1994).
39. Kresse, G. & Joubert, D. From Ultrasoft Pseudopotentials to the Projector Augmented-Wave Method. *Phys. Rev. B* **59**, 1758–1775 (1999).
40. Kresse, G. & Furthmüller, J. Efficiency of ab-initio Total Energy Calculations for Metals and Semiconductors Using a Plane-Wave Basis Set. *Comp. Mater. Sci.* **6**, 15–50 (1996).
41. Kresse, G. & Furthmüller, J. Efficient Iterative Schemes for ab initio Total-Energy Calculations Using a Plane-Wave Basis Set. *Phys. Rev. B* **54**, 11169–11186 (1996).
42. Perdew, J. P., Burke, K. & Ernzerhof, M. Generalized Gradient Approximation Made Simple. *Phys. Rev. Lett.* **77**, 3865–3868 (1996).
43. Dudarev, S. L., Botton, G. A., Savrasov, S. Y., Humphreys, C. J. & Sutton, A. P. Electron-Energy-Loss Spectra and the Structural Stability of Nickel Oxide: An LSDA + *U* Study. *Phys. Rev. B* **57**, 1505–1509 (1998).
44. Mostofi, A. A. *et al.* wannier90: A Tool for Obtaining Maximally-Localised Wannier functions. *Comput. Phys. Commun.* **178**, 685–699 (2008).
45. Marzari, N., Mostofi, A. A., Yates, J. R., Souza, I. & Vanderbilt, D. Maximally Localized Wannier Functions: Theory and Applications. *Rev. Mod. Phys.* **84**, 1419–1475 (2012).
46. Ferreira, L. G., Wei, S. H. & Zunger, A. First-principles Calculation of Alloy Phase Diagrams: The Renormalized-Interaction Approach. *Phys. Rev. B* **40**, 3197–3231 (1989).
47. van de Walle, A., Asta, M. & Ceder, G. The Alloy Theoretic Automated Toolkit: A User Guide. *Calphad.* **26**, 539–553 (2002).
48. Hukushima, K. & Nemoto, K. Exchange Monte Carlo Method and Application to Spin Glass Simulations. *J. Phys. Soc. Jpn.* **65**, 1604–1608 (1996).
49. Wang, P. S., Ren, W., Bellaiche, L. & Xiang, H. J. Predicting a Ferrimagnetic Phase of $\text{Zn}_2\text{FeOsO}_6$ with Strong Magnetoelectric Coupling. *Phys. Rev. Lett.* **114**, 147204 (2015).

Acknowledgements

This work was supported by NSFC (11374056), the Special Funds for Major State Basic Research (2012CB921400, 2015CB921700), Program for Professor of Special Appointment (Eastern Scholar), Fok Ying Tung Education Foundation, FANEDD, and NCET-10-0351.

Additional Information

Supplementary information accompanies this paper at <http://www.nature.com/srep>

Competing financial interests: The authors declare no competing financial interests.

How to cite this article: Liu, K. *et al.* Orbital Delocalization and Enhancement of Magnetic Interactions in Perovskite Oxyhydrides. *Sci. Rep.* **6**, 19653; doi: 10.1038/srep19653 (2016).



This work is licensed under a Creative Commons Attribution 4.0 International License. The images or other third party material in this article are included in the article’s Creative Commons license, unless indicated otherwise in the credit line; if the material is not included under the Creative Commons license, users will need to obtain permission from the license holder to reproduce the material. To view a copy of this license, visit <http://creativecommons.org/licenses/by/4.0/>